ChemComm

Accepted Manuscript

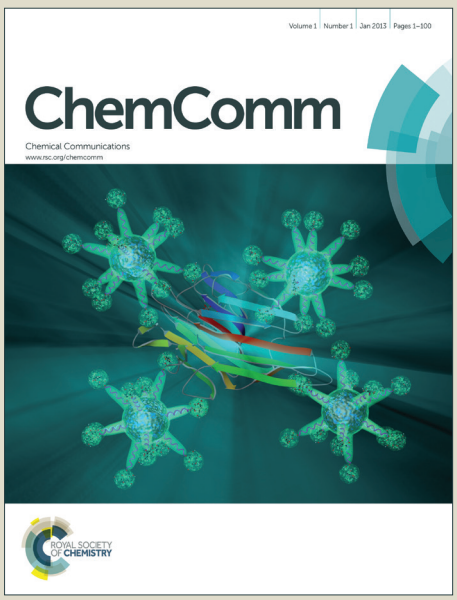

ROYAL SOCIETY OF CHEMISTRY

www.rsc.org/chemcomm

Cite this: DOI: 10.1039/c0xx00000x

www.rsc.org/xxxxxx

ARTICLE TYPE

Sub-5 nm nanobowl gaps electrochemically templated by SiO_2-coated Au nanoparticles as surface-enhanced Raman scattering hot spots

Haiqiong Wen,[a] Lingyan Meng,[b] Gezhi Kong,[a] Huimin Yu,[a] Zhilin Yang,*[b] and Jiawen Hu*[a]

Received (in XXX, XXX) Xth XXXXXXXXX 20XX, Accepted Xth XXXXXXXXX 20XX

DOI: 10.1039/b000000x

Large-area submonolayer and monolayer Au nanoparticle (NP) arrays around with sub-5 nm nanobowl gaps for giant electromagnetic enhancement were created by partially embedding SiO_2-coated Au NP arrays in an electrochemically deposited Au film, followed by removal of the SiO_2 shells.

In surface-enhanced Raman scattering (SERS), nanometer gap junctions between particles and sharp surface protrusions, known as "hot spots", can create extremely intense local electromagnetic (EM) fields and thus are essential for the enormous SERS enhancements.[1, 2] For example, a recent research reveal that 63 sites of 1,000,000 SERS-active sites contribute 24% of the total SERS intensity.[3] Together with this giant enhancement, the "hot spots" also result in very large variation in SERS signal because for most roughened SERS substrates commonly employed, they are randomly distributed and uncontrollable. This poor spectral reproducibility is one of the main drawbacks that hinder the widespread applications of SERS.

Over the past decades, great efforts have been devoted for the construction of "hot spots" in order to maximize SERS enhancements. Recent achievements and advances include templated NP arrays,[4, 5] salt-[6, 7] or functional molecule-[8, 9] induced NP aggregates, self-assembled NP dimmers[10] or arrays,[11] chemically driven NP assembly,[12, 13] thermosensitive NP assembly,[14] lithography-engineered arrays,[15, 16] bilayered Au nanostructures,[17] individual nanometer hole-particle pairs,[18] and mechanically controllable break-junction.[19] However, the preparation of a SERS substrate with abundant, easy-to-construct, and reproducible nanogaps still faces a great challenge due to complex preparation processes and high cost.

Nanosphere lithography is a well-established technique that utilizes monolayer colloidal crystal as a lithographic mask to construct structured nanostructures.[20, 21] Very recently, we used the polystyrene sphere monolayer to template structured Au sphere segment void (SSV) substrates for the application of borrowed SERS.[22] Inspired by the template idea, here, we further utilize SiO_2-coated Au ($Au@SiO_2$) NP arrays as the template to create reproducible sub-5 nm nanobowl gaps around Au NP arrays. This method allows us to take advantages of routine NP synthesis and electrodeposition techniques to create nanometer sized gaps that is beyond the current lithography. Furthermore, the open bowled gaps largely increase the volume of the hot spots, which allows more molecules to be loaded, thereby may generate new spectral characteristics for SERS substrate.

Fig. 1 shows the preparation process for the nanobowl gaps, which involved assembly of $Au@SiO_2$ NP arrays on a conductive Au surface (denoted as Au substrate hereafter), electrodeposition of Au through the arrays, and removal of the SiO_2 shells. The synthesis of $Au@SiO_2$ NPs with a 55 nm Au core and a < 5-nm thick SiO_2 shell was following the reported method.[23,24] After synthesis, cyclic voltammetry and SERS tests were performed to diagnose the pinholes on the shell of the $Au@SiO_2$ NPs.[24] Only pinhole-free $Au@SiO_2$ NPs that show no Au oxide stripping peak and no SERS peaks (Fig 2S† and Fig 3S†) were chosen. Such an examination and the insulated nature of SiO_2 insure that the Au deposit film grows around, instead covers, the $Au@SiO_2$ template NPs during the following electrodeposition.

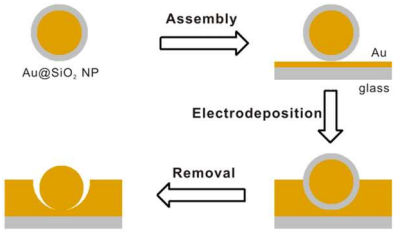

Fig. 1 Schematic illustration of the preparation flow of the Au NP arrays around with sub-5 nm nanobowl gaps

Submonolayer $Au@SiO_2$ NP arrays were assembled on the Au substrate by immersing the 3-aminopropyltrimethoxysilane-functionalized substrate in the $Au@SiO_2$ aqueous solution; whilst monolayer $Au@SiO_2$ NP arrays were first assembled at a water-air interface followed by transferring them onto the Au substrate (the preparation processes for both arrays are detailed in the ESI†). Fig 2A and Fig S4A† show the SEM images of the submonolayer and monolayer $Au@SiO_2$ NP arrays assembled on the Au substrate, respectively. In the submonolayer arrays, the $Au@SiO_2$ NPs are randomly distributed with each particle circled by a clear light layer of about 4 nm thickness, *i.e.*, the SiO_2 shell. In contrast, the $Au@SiO_2$ NPs are closely packed in the monolayer arrays. Au was deposited through the $Au@SiO_2$ NP arrays using a commercial Au plating solution TSG-250 at a constant current of 10 $\mu A \cdot cm^{-2}$. A 32-nm thick Au film was deposited by monitoring the charge passed during electrodeposition and employing 70% efficiency for the electrodeposition. Fig. 2B and Fig. S4B† show that the surface of electrochemically deposited Au film is smooth, in which the $Au@SiO_2$ NPs are, as expected, partially embedded. Successful

template construction of the nanobowl gaps requires the Au deposit film to be thinner than the diameter of the template NP and be smooth as possible. However, at such a small thickness, the surface roughness of the underneath Au substrate, which were prepared by vacuum evaporation, would unavoidably be transferred to the thin Au film deposited. We originally used home-made Au plating solution, but only achieved a rough, non-uniform Au deposit film. It is known from electrodeposition science that plating solution added with special additives has excellent throwing power and levelling effect, i.e., ability to deposit metals uniformly and natural ability to level the imperfects on an irregular surface. After trying a few commercial Au plating solutions, we found that TSG-250 allows us to achieve the desired smooth, flat Au deposit film.

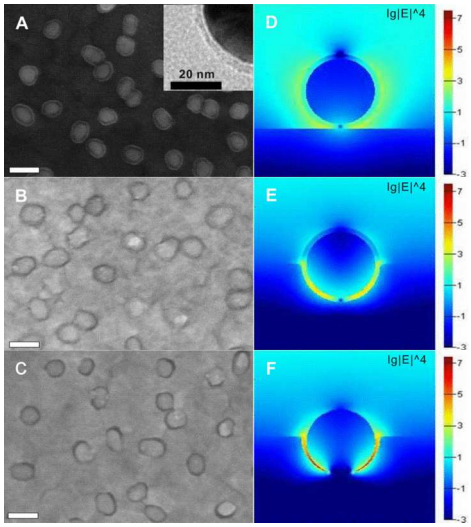

Fig. 2 SEM images (A-C) and corresponding EM field distribution (D-F) of submonolayer Au@SiO_2 NP arrays on an Au surface before electrodeposition (A, D), after electrodeposition of a 32 nm-thick Au film (B, E), and upon removal of the silica shells (C, F). The inset in image A is the magnified TEM image intended to show the shell of the Au@SiO_2 NP. Scale bars are 100 nm.

Following electrodeposition, the SiO_2 shell was removed by dissolving the SiO_2 shell in a 5 M NaOH solution. The higher magnified SEM images, shown in Fig. 2C and Fig. S4C†, clearly reveal that nanobowl gap is created around each particle in the arrays. To further demonstrate the successful creation, Fig. S5† shows the lower SEM images for both submonolayer and monolayer arrays before and after the removal of the SiO_2 shell. The smooth surface for the Au deposit film is retained after removal of the SiO_2 shell in severe alkaline conditions, thereby largely restraining the contributions coming from non-uniform surface morphology, beside the desired nanobowl gaps, to the observed SERS intensity. For templated gaps, their resolutions in *x*- and *y*-directions are determined by the shell size of the Au@SiO2 NPs, thereby can achieve a nanometer resolution because present NP synthesis techniques allow controlling NP size in nanometer precision. The resolution in the *z*-direction is determined by the height of the deposit, which could even achieve an atomic layer precision if atomic layer deposition technique, e.g., underpotential deposition,[25] was used. Ideally, a deposited film with a flat surface finish and precisely controlled thickness is highly desired for the preparation of templated nanogaps with high resolution.

To establish the SERS behaviour of the Au NP arrays around with sub-5 nm nanobowl gaps, 4-mercaptobenzoic acid (4-MBA) was used as a probe molecule, which was adsorbed on the arrays by immersing the arrays in 1 mM 4-MBA solution in ethanol for 30 minutes. Fig 3 and Fig S6† show that the SERS intensities are negligible for the exposed submonolayer and monolayer Au@SiO_2 NP arrays. After partially embedding the arrays in the Au deposit film, the SERS intensities on the two Au NP arrays around with sub-5 nm nanobowl gaps are much strong, about 7 times than that on their corresponding arrays without the gaps, thereby confirming 85% contributions from the gaps created. The strong SERS peaks at 1077 and 1587 cm^{-1} are, respectively, assigned to the ν_{12} and ν_{8a} vibration modes of the aromatic ring;[26] whilst the other three moderately strong peaks appeared at 689, 998, and 1020 cm^{-1} are characteristics of monosubstituted benzene derivatives.[27] For the two arrays around with sub-5 nm nanobowl gaps, their averaged enhancement factors are estimated to be 2.5×10^5 and 1.94×10^5, respectively (for details, see ESI†). To further reveal the regional intensity variation, SERS measurements were measured across the two arrays for 20 times. Fig. S7† and Fig. S8† indicates that the spectral variations on the two arrays are, respectively, less than 17.3% and 5.2%. As the two arrays are not structured surfaces, their unexpected good spectral reproducibility can only be attributed to a large increase in hot spot density (or hot spot volume), which averages the variation in SERS intensity and thus improve spectral reproducibility.

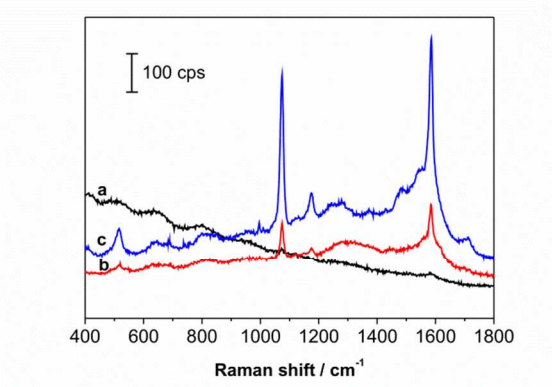

Fig. 3 SERS spectra of 4-MBA adsorbed on the submonolayer Au@SiO_2 NP arrays before electrodeposition (a), after electrodeposition of a 32 nm-thick Au film (b), and upon removal of the silica shells (c). Excitation line: 632. 8 nm; accumulation time: 10 s. To avoid laser burning the molecule, its intensity is attenuated to an extent that the intensity of the 520 cm^{-1} peak of silicon for a single 1-s accumulation is 423 cps.

The EM fields generated by the related nanostructured surfaces are inherent to the SERS behaviours observed above. To quantitatively understand the SERS behaviours, theoretical simulations were performed using a three-dimensional finite-difference time-domain (3D-FDTD) method, as are detailed in the ESI†. To conveniently determine the order of enhancement and find the location of the hot spots, near field enhancement distributions of $|E|^4$ are shown under logarithmic coordinates and are normalized by the fourth power of the electric field of the incident wave at the position of the molecule. Enhancement factor for SERS is proportional to E^4, where E represents the field

enhancement defined as the ratio of the local field E_{loc} to the incoming field E_{in}, $E = |E_{loc}|/|E_{in}|$. Before electrodeposition, the Au@SiO_2 NP arrays were exposed on the supporting Au substrate. The hot spots locate at the junctions between the Au@SiO_2 NPs and the underneath Au substrate (Fig. 2D and Fig. S4D†), where the enhancement factors achieve the maximum values of 2.5×10^3 and 3.2×10^4 for the submonolayer and monolayer Au@SiO_2 NP arrays, respectively. Molecules placed in these hot spots would experience SERS enhancement, known as shell-isolated nanoparticle-enhanced Raman spectroscopy established by Tian group in 2010.[24] In our case, the 4-MBA molecules were hindered to enter the hot spots by the APTS layer, which was modified on the Au substrate for anchoring the Au@SiO_2 NPs, and, as well, isolated from the Au core by the pinhole-free SiO_2 shell so that their SERS peaks are rather weak (curves a in Fig. 3 and Fig. S6†). After electrodeposition, the Au@SiO_2 NP arrays were partially embedded in the Au deposit film. In this case, the hot spots locate in the silica layer between the Au NP and the Au deposit film (Fig. 2E and Fig. S4E†), and the maximum enhancement factors reach 4.0×10^4 and 1.6×10^4 for the submonolayer and monolayer Au@SiO_2 NP arrays, respectively. As the hot spots is in inaccessible for the probe molecules, the weak SERS signals (curves b in Fig. 3 and Fig. S6†) should be contributed by the imperfections on the Au deposit film, which are unable to be eliminated completely even using high quality commercial Au plating solution. Upon removal of the SiO_2 shell, the enhanced EM field is concentrated in the nanobowl gap particularly at its bottom. The calculated maximum SERS enhancements for the submonolayer and monolayer Au NP arrays are as high as 2.5×10^7 and 1.0×10^6, respectively, which are 1-2 orders larger than the enhancements obtained in the experimental systems. Considering the surface averaged SERS enhancement is often 1-2 orders lower than the maximum value,[3, 28] the calculated EFs are thus in good agreement with the EFs experimentally determined because the later are the averaged EFs over the entire surface. To direct choosing NPs that are able to template nanobowl gaps with giant EM fields, theoretical simulations were further performed for a series of nanobowl gaps made from the arrays of different shell thickness. Fig. S9† shows that when the shell thickness decreases from 4 to 3, 2, and 1 nm, the maximum enhancement factor for the templated nanobowl gaps gradually decreases from 2.5×10^7 to 1.0×10^7, 1.3×10^6, and 2.0×10^5. Therefore, the undesignedly chosen Au@SiO_2 NPs with a 4 nm shell are the best choice among the four sorts of Au@SiO_2 NPs examined for templating the nanobowl gaps.

In summary, we template sub-5 nm nanobowl gaps from the Au@SiO_2 NPs with a < 5 nm shell taking advantages of NP synthesis and electrodeposition techniques. Compared with the small exterior "hot spots" between adjacent NPs, the open nanobowl gaps not just produce giant EM enhancements. They, as well, largely increase the volume for the hot spots to load a more amount of Raman dyes, thereby averaging the large signal variation commonly observed on a disordered SERS substrate. The method described here opens avenues for the creation of gaps of only a few nanometers using routine laboratory techniques, which may find widespread applications in SERS and other fields, *e.g.*, molecular electronics.

This work was financially supported by the National Natural Science Foundation of China (Grant Nos. 20873037, 91027037, J1103312, J1210040, 21173171, and 11074210)

Notes and references

[a] *State Key Laboratory for Chemo/Biosensing and Chemometrics, and College of Chemistry and Chemical Engineering, Hunan University, Changsha, 410082, China. Fax: +86-731-85956121; E-mail: jwhu@hnu.edu.cn*

[b] *Department of Physics, Xiamen University, Xiamen 361005, China E-mail: zlyang@xmu.edu.cn*

† Electronic Supplementary Information (ESI) available: Experimental section, details for 3D-FDTD simulations and evaluation of enhancement facor, and supplementary results of UV-Vis, CV, SEM, 3D-FDTD simulations, and SERS spectra. See DOI: 10.1039/b000000x/

1. H. Xu, J. Aizpurua, M. Käll and P. Apell, *Physical Review E*, 2000, **62**, 4318.
2. H. Xu, E. J. Bjerneld, M. Käll and L. Börjesson, *Phys. Rev. Lett.*, 1999, **83**, 4357.
3. Y. Fang, N.-H. Seong and D. D. Dlott, *Science*, 2008, **321**, 388.
4. P. Nielsen, S. Hassing, O. Albrektsen, S. Foghmoes and P. Morgen, *J. Phys. Chem. C*, 2009, **113**, 14165.
5. H. H. Wang, C. Y. Liu, S. B. Wu, N. W. Liu, C. Y. Peng, T. H. Chan, C. F. Hsu, J. K. Wang and Y. L. Wang, *Adv. Mater.*, 2006, **18**, 491.
6. J. Chen, B. Shen, G. Qin, X. Hu, L. Qian, Z. Wang, S. Li, Y. Ren and L. Zuo, *J. Phys. Chem. C*, 2012, **116**, 3320.
7. W. Li, P. H. C. Camargo, X. Lu and Y. Xia, *Nano Lett.*, 2008, **9**, 485.
8. D.-K. Lim, K.-S. Jeon, H. M. Kim, J.-M. Nam and Y. D. Suh, *Nat. Mater.*, 2009, **9**, 60.
9. M. M. Maye, D. Nykypanchuk, M. Cuisinier, D. van der Lelie and O. Gang, *Nat. Mater.*, 2009, **8**, 388.
10. H. Guo, D. Jiang, H. Li, S. Xu and W. Xu, *J. Phys. Chem. C*, 2012, **117**, 564.
11. H. Wang, C. S. Levin and N. J. Halas, *J. Am. Chem. Soc.*, 2005, **127**, 14992.
12. G. Braun, I. Pavel, A. R. Morrill, D. S. Seferos, G. C. Bazan, N. O. Reich and M. Moskovits, *J. Am. Chem. Soc.*, 2007, **129**, 7760.
13. G. Chen, Y. Wang, M. Yang, J. Xu, S. J. Goh, M. Pan and H. Chen, *J. Am. Chem. Soc.*, 2010, **132**, 3644.
14. Y. Wu, F. Zhou, L. Yang and J. Liu, *Chem. Commun.*, 2013, **49**, 5025.
15. H. Duan, H. Hu, H. K. Hui, Z. Shen and J. K. Yang, *Nanotechnology*, 2013, **24**, 185301.
16. H. Im, K. C. Bantz, S. H. Lee, T. W. Johnson, C. L. Haynes and S.-H. Oh, *Adv. Mater.*, 2013, **25**, 2678.
17. D.-K. Lim, K.-S. Jeon, J.-H. Hwang, H. Kim, S. Kwon, Y. D. Suh and J.-M. Nam, *Nat. Nanotechnol*, 2011, **6**, 452.
18. H. Wei, U. Håkanson, Z. Yang, F. Höök and H. Xu, *Small*, 2008, **4**, 1296.
19. J.-H. Tian, B. Liu, Li, Z.-L. Yang, B. Ren, S.-T. Wu, Tao and Z.-Q. Tian, *J. Am. Chem. Soc.*, 2006, **128**, 14748.
20. K. A. Willets and R. P. Van Duyne, *Annu. Rev. Phys. Chem.*, 2007, **58**, 267.
21. S. Cintra, M. E. Abdelsalam, P. N. Bartlett, J. J. Baumberg, T. A. Kelf, Y. Sugawara and A. E. Russell, *Faraday Discuss.*, 2006, **132**, 191.
22. J. Hu, S. Chen, R. P. Johnson, X. Lin, Z. Yang and A. E. Russell, *J. Phys. Chem. C*, 2013, **117**, 24843.
23. L. M. Liz-Marzán, M. Giersig and P. Mulvaney, *Langmuir*, 1996, **12**, 4329.
24. J. F. Li, Y. F. Huang, Y. Ding, Z. L. Yang, S. B. Li, X. S. Zhou, F. R. Fan, W. Zhang, Z. Y. Zhou and D. Y. Wu, *Nature*, 2010, **464**, 392.
25. E. Herrero, L. J. Buller and H. D. Abruña, *Chem. Rev.*, 2001, **101**, 1897.
26. H. Park, S. B. Lee, K. Kim and M. S. Kim, *J. Phys. Chem.*, 1990, **94**, 7576.
27. F. R. Dollish, W. G. Fateley and F. F. Bentley, *Characteristic Raman frequencies of organic compounds*, Wiley New York, 1974.162-190.
28. S. L. Kleinman, R. R. Frontiera, A.-I. Henry, J. A. Dieringer and R. P. Van Duyne, *Phys. Chem. Chem. Phys.*, 2013, **15**, 21.